

# Preparation of Metal–Organic Frameworks UiO-66 for Adsorptive Removal of Methotrexate from Aqueous Solution

Mozhgan Aghajanzadeh<sup>1</sup> · Mostafa Zamani<sup>1</sup> · Hossein Molavi<sup>2</sup> ·  
Hamidreza Khieri Manjili<sup>3,4</sup> · Hossein Danafar<sup>3,5,6,7</sup> · Akbar Shojaei<sup>8</sup>

Received: 10 August 2017 / Accepted: 17 October 2017 / Published online: 26 October 2017  
© Springer Science+Business Media, LLC 2017

**Abstract** A low cytotoxic metal–organic framework (MOF) UiO-66 (UiO stands for University of Oslo) and NH<sub>2</sub>-UiO-66, that showed high cell viability of HFF-2 via 3-(4, 5-dimethylthiazol-2-yl) 2, 5-diphenyl tetrazolium assay, was reported as an effective adsorbent (antidotal) agents. The structure of MOFs was confirmed by Fourier transform infrared, Field emission scanning electron microscopy (FESEM) and X-ray diffraction. Thermal behavior of MOFs was investigated using with thermogravimetric analyzer in nitrogen atmosphere to check the thermal stability. FESEM showed NH<sub>2</sub>-UiO-66 displayed symmetrical crystals with triangular base pyramid morphology, with

the particle size around 100 nm and uniform size distribution. The specific surface areas were calculated using the Brunauer–Emmett–Teller method and surface area and total pore volume of NH<sub>2</sub>-UiO-66 were calculated to be 1258 m<sup>2</sup>/g and 0.51 cm<sup>3</sup>/g, respectively. Methotrexate salt (MTX) was selected as the model drug which was adsorbed into inner pores and channels of MOFs by diffusion manner. The interaction between MOFs and MTX and the effect of pH on interaction between them in aqueous solution was investigated. The final results showed that UiO-66 have high adsorbing capacity and great affinity to MTX.

**Keywords** Mesoporous · Metal organic framework · Antidote · Methotrexate

✉ Hossein Danafar  
danafar@zums.ac.ir

✉ Akbar Shojaei  
akbar.shojaei@sharif.ir

<sup>1</sup> Department of Pharmaceutical Biomaterials, School of Pharmacy, Zanjan University of Medical Sciences, Zanjan, Iran

<sup>2</sup> Institute for Nanoscience and Nanotechnology (INST), Sharif University of Technology, Tehran, Iran

<sup>3</sup> Department of Pharmaceutical Nanotechnology, School of Pharmacy, Zanjan University of Medical Sciences, Zanjan, Iran

<sup>4</sup> Zanjan Pharmaceutical Biotechnology Research Center, Zanjan University of Medical Sciences, Zanjan, Iran

<sup>5</sup> Zanjan Pharmaceutical Nanotechnology Research Center, Zanjan University of Medical Sciences, Zanjan, Iran

<sup>6</sup> Department of Medicinal Chemistry, School of Pharmacy, Zanjan University of Medical Sciences, Zanjan, Iran

<sup>7</sup> Cancer Gene Therapy Research Center, Zanjan University of Medical Sciences, Zanjan, Iran

<sup>8</sup> Department of Chemical and Petroleum Engineering, Sharif University of Technology, Tehran, Iran

## 1 Introduction

In all cases, overdose of drugs and addiction can lead claiming of lives, the destroying and decreasing the quality of life around the world. Many people die every year because of overdose. This is the main cause of death in people who taking injecting medications [1]. according to the evidences, for over a decade unwitting drug overdose have been growing problems across the world [2].

By using a chemotherapy method with new drug delivery methods, the goal of the pharmaceutical scientist is to increase the therapeutic efficacy and reduce the possibility of drug's side effects. Methotrexate (MTX) is used to treat cancer, induction of abortion with misoprostol and autoimmune diseases. Research has shown that aminotherm (a folic acid analog discovered (1947) by Yellapragada Subbarao), can be used for children with acute lymphoblastic leukemia. Progress in the synthesis of folic acid analogs was continued based on the fact that folic acid supply could worsen the

leukemia and deficiency of folic acid improve the treatment action of folic acid analogs. In 1950, MTX (formerly introduced as amethopterin) was used instead of aminopterin, the most toxic antitumor treatment for leukemia [3].

Metal–organic frameworks (MOFs) are the last class of solid porous composite compounds discovered in 1989 by Robson [4]. Due to this, many applications have been proposed for it, such as adsorption, storage, separation, ion exchange, drug delivery, catalysis, magnetism and health care applications [5–14]. One of their main advantages is the possibility to easily tune their composition using a change in the organic linker and/or the metal which compared to organic (carbons) or inorganic counterparts (zeolites, silica), is an advantage. Possible linkers are very varied, ranging from sulfonates, polycarboxylates, phenolates, amines, pyridyl. So, thousands of MOFs have been synthesized with at least a few hundreds of them that being porous to nitrogen gas. Compared with zeolites, MOFs have a wider chemical versatility and exhibit a larger panel of shapes and pore sizes (tunnels, cages, etc.), with most of the time a flexible porosity that allows to reversibly adapt the pore size to the adsorbate [15]. Functionalization of the organic linker bring other benefits of MOFs which make grafting during or after the synthesis various organic functionalities and changing thus the physicochemical properties of the solid [16]. Whether compound has a biomedical application [17], depends on several parameters such as the application, the balance between risk and benefit, and the kinetics of degradation, bio-distribution, accumulation in tissues and organs and excretion from the body and so on. Due to their low toxicity, MOFs can be used for biomedical applications.

MOFs have a large capacity to adsorb toxins [18, 19], a lot of research has been done in this field in recent years. Up to now, many adsorbent materials such as activated carbon [20] and zeolites [21] have been widely used for the removal/adsorption of different industrial dyes and wastes. It's interesting that industrial wastes such as solid wastes [22], banana and orange peel [23] have also been used as adsorbents. In addition, magnetic particles have been dispersed/incorporated in the adsorbent solution to separate adsorbent from liquid [23].

However, there has not report of using UiO-66 MOF in the removal of MTX. In related to our previous work to design and preparation of various type of nanoparticles for drug delivery and adsorbent systems [24–34]. In this study, for the first time, we report the adsorption of hydrophilic MTX salt by MOFs, especially well-studied UiO-66 and NH<sub>2</sub>-UiO-66, for understanding the characteristics of adsorption and using MOFs as adsorbents for the removal of some drugs from body. Previous researches showed that addition of amine group to chemical compound like chitosan can improve antibacterial activity [35], so with this method, adsorbent become more resistant to microorganisms. Finally,

to make sure the safety of adsorbent agents, their toxicity was measured on normal cells Human foreskin fibroblast (HFF2) using (3-[4, 5-dimethylthiazol-2-yl]-2, 5-diphenyltetrazolium bromide, Sigma) MTT assay.

## 2 Materials and Methods

### 2.1 Material

2-aminoterephthalic acid (2-ATA 99%) and zirconium chloride (ZrCl<sub>4</sub>, 99.9%) were obtained from Sigma-Aldrich. Terephthalic acid (BDC 99%) was supplied by Merck. All other solvents and reagents of analytical grade were purchased from Merck, and were used as received without further purification. All solutions were prepared with distilled and double distilled water.

### 2.2 Preparation of Antidotal Agents

UiO-66 was prepared according to the procedure reported in previous studies [25, 36]. 0.53 g of zirconium (IV) chloride (ZrCl<sub>4</sub>) was completely dissolved in 30 mL of DMF at room temperature and stirred vigorously until a clear solution was formed. 0.38 g of terephthalic acid was added to the homogenous solution and stirred for 1 h. Subsequently, the homogenous solution was transferred to a 50 mL Teflon-lined autoclave and was placed in a preheated oven to allow crystal growth at 120 °C for 24 h. The product obtained was collected by centrifuge and washed three times with DMF and three times with chloroform under sonication for 10 min to remove the unreacted reactants. The solid was solvent exchanged by soaking for 5 days in 2 × 15 of chloroform followed by sonication for 10 min. Finally the white powder was dried at 100 °C under dynamic vacuum for 24 h to remove the solvents from the pores. NH<sub>2</sub>-UiO-66 was prepared in accordance with the same procedure and using 2-aminoterephthalic acid (0.41 g) instead of terephthalic acid.

### 2.3 Characterization of Antidotal Agents

Fourier transform infrared (FTIR) spectra were recorded on a 100-FT-IR Spectrometer, Perkin-Elmer. The spectra were scanned from 500 to 4000 cm<sup>-1</sup> with a wavenumber resolution of 4 cm<sup>-1</sup>. The PXRD features of UiO-66 and NH<sub>2</sub>-UiO-66 were determined by X-ray diffraction on an X-pert Philips, pw 3040/60 diffractometer at 40 kV and 40 mA, with a scan rate of 0.026°/s in 2θ = 3°–50°, using Cu K<sub>α1</sub> radiation (λ = 1.54060 Å). The thermal stability of two MOFs was investigated by Thermogravimetric analysis using Perkin-Elmer Pyris thermogravimetric analyzer (TGA). The MOFs were heated from 25 to 800 °C at a heating rate of 10 °C/min under nitrogen atmosphere. Field

emission scanning electron microscopy was conducted on a FESEM–MIRA3 TESCAN. The nitrogen adsorption/desorption isotherms of UiO-66 and NH<sub>2</sub>-UiO-66 were collected using BELSORP-miniII adsorption porosimeter at 70 K after being degassed at 150 °C under vacuum overnight. The specific surface areas were calculated using the Brunauer–Emmett–Teller (BET) method, the total pore volumes were determined at a relative pressure of 0.99, and the pore size distributions were calculated according to the Barrett–Joyner–Halenda method from the adsorption branch.

## 2.4 Analysis of Antidotal Potency of MOFs

### 2.4.1 Adsorption Experiments

To evaluate the adsorption capacity, 60 mg of UiO-66 and NH<sub>2</sub>-UiO-66 were dispersed in 50 mL of MTX solutions at different concentrations (from 0.24 to 0.96 mg mL<sup>-1</sup>), then the solutions were kept in room temperature and stirred for 2 h. At the end of the work, the solution was centrifuged for 15 min, and Ultraviolet spectroscopy (UV–Vis) was used to measure the residual concentrations of MTX. The equilibrium adsorption capacity  $Q_e$  (mg g<sup>-1</sup>) was calculated according to Eq. [26]:

$$Q_e = \frac{(C_0 - C_e)V}{M} \quad (1)$$

where  $C_0$  and  $C_e$  (mg mL<sup>-1</sup>) were the initial and equilibrium concentrations of MTX, respectively.  $V$  (mL) was the volume of the solution, and  $M$  (g) was the mass of adsorbent.

### 2.4.2 Kinetic Study

For the kinetic studies, exactly 5 mg of each MOFs were added into a series of 15 mL Conical Centrifuge Tubes containing 5 mL of 400 µg mL<sup>-1</sup> MTX. The tubes were shaken at 300 rpm at 310 K, and one tube was taken out and filtered at preset time intervals to analyze the solute concentration in the filtrate. The tubes were centrifuged at 4000 rpm and 1 mL of supernatant was collected. The concentrations of MTX were analyzed by UV–Vis at 306 nm.

### 2.4.3 Methotrexate Release Study

The effect of pH on the interaction between MOFs and the drug was studied by release mode experiment. To study the effect of pH on the interaction between MOFs and the drug in aqueous solutions, 5.0 mg of MOFs containing drug was dispersed in 2 mL of phosphate buffer saline (PBS) solution, with pH to 5 and 7.4. The solution was placed in dialysis bag and incubated at 37 °C while immersed in 20 mL PBS. After predetermined time 1 mL of dialysate was collected and replaced by 1 mL of fresh PBS. UV–Vis

spectroscopy was used to measure the concentrations of MTX from supernatant.

### 2.4.4 Cell Cytotoxicity

HFF2 cells were cultured in 96-well plates and were treated by antidotal agents (MOFs). After 24 and 48 h incubation, the cell viability was measured via MTT assays. In brief, cells were plated in a 96-well plate (5 × 10<sup>4</sup> cells/well) in 100 µL of Dulbecco's Modified Eagle medium (DMEM) containing 15% FBS and 1% penicillin and streptomycin for 24 h. 100 µL of MOFs dispersion in DMEM at varying MOFs concentrations from 30 to 710 µg/mL were added. The cells were cultured at 37 °C under an atmosphere containing 5% CO<sub>2</sub> for another 72 h. Then, 10 µL of MTT solution in PBS (5.0 mg/mL) was added and incubated for another 4 h at 37 °C. The medium was aspirated, and the MTT-formazan generated by live cells was dissolved in 100 µL of DMSO. Absorbance readings of each well were performed at 570 nm (single wavelength) using a multi scan plate reader made in the UK. The cell viability (%) was determined by comparing the absorbance at 570 nm with control wells containing only cell culture medium. Data are presented as mean ± SD (n = 3).

## 3 Results and Discussion

### 3.1 Characterization of MOFs

#### 3.1.1 FT-IR

The FTIR spectra of UiO-66 and NH<sub>2</sub>-UiO-66 activated by chloroform are presented in Fig. 1. As shown in Fig. 1, it can be seen that MOF particles have some characteristic peaks at the range of 1400–1700 cm<sup>-1</sup>, which are attributed to stretching vibrations of C=C and C=O bonds. The weak bands (2850–3100 cm<sup>-1</sup>) which observed the spectra of two MOFs are attributed to the aromatic and aliphatic stretching (C–H) modes of benzene and DMF [37]. The strong and broad absorption band observed in the range of 3200–3600 cm<sup>-1</sup> could be due to the presence of hydrogen bonded water molecules physisorbed on the surface or inter crystalline water. Two characteristic peaks observed at 3376 and 3457 cm<sup>-1</sup>, indicating the presence of the NH<sub>2</sub> group as well as the 2-aminoterephthalic acid in the NH<sub>2</sub>-UiO-66. Because of overlap between these peaks and the OH groups, distinction of two peaks not completely possible. Comparison FTIR spectra of the samples after inclusion of MTX with the pristine samples showed that, the intensity of absorption band at around 2850–2950 cm<sup>-1</sup> increased, which could be attribute to the aliphatic C–H groups of MTX. Therefore, the FTIR spectra showed that the MTX successfully adsorb on the surface of MOFs.

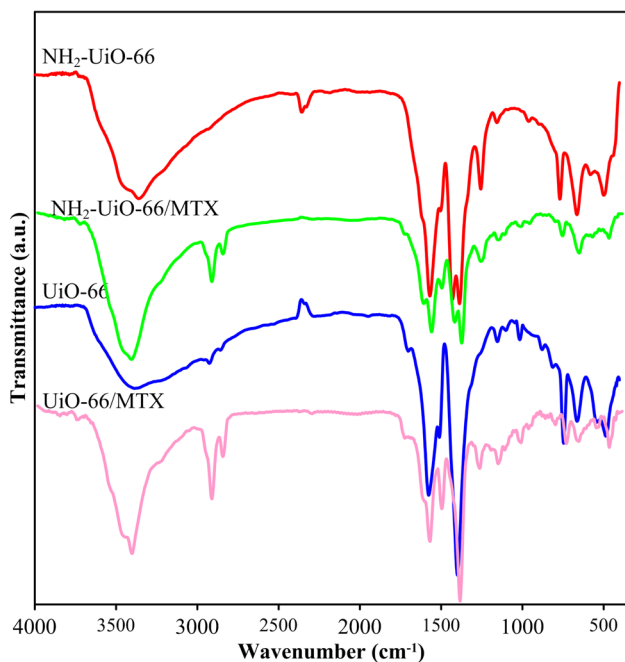


**Fig. 1** FTIR spectra of UiO-66, NH<sub>2</sub>-UiO-66 and the samples after inclusion of MTX

### 3.1.2 XRD

The XRD pattern of UiO-66 and NH<sub>2</sub>-UiO-66 are given in Fig. 2. The characteristic peaks of UiO-66 and NH<sub>2</sub>-UiO-66, which are shown inside the figure matched well with the

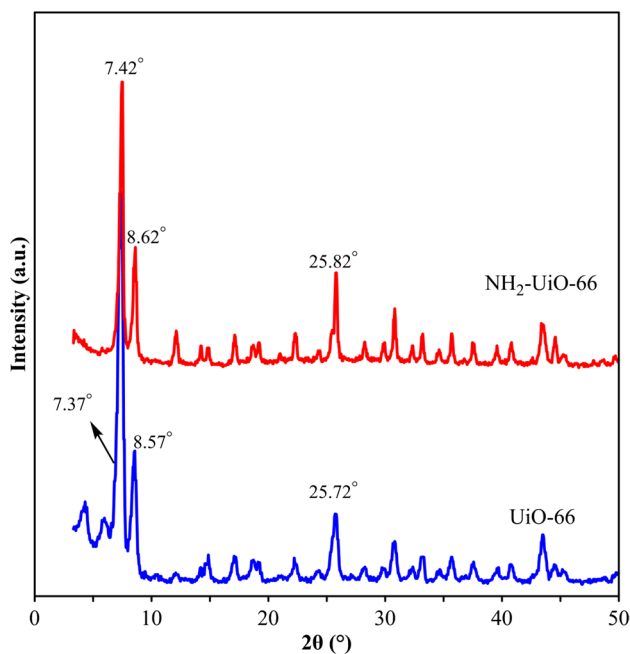


**Fig. 2** XRD patterns of UiO-66 and NH<sub>2</sub>-UiO-66

XRD patterns previously reported [8]. The appearance of sharp peaks in the XRD patterns of samples is an evidence of good degree of crystallinity in prepared MOFs. The results indicate that UiO-66 and NH<sub>2</sub>-UiO-66 were well prepared, and there is not any impurity in the structure of them [38, 39].

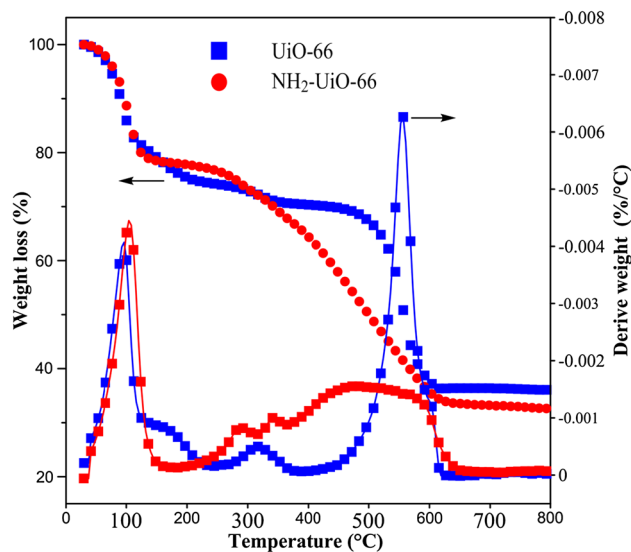


**Fig. 3** TGA and derivative TG (DTG) curves of UiO-66 and NH<sub>2</sub>-UiO-66

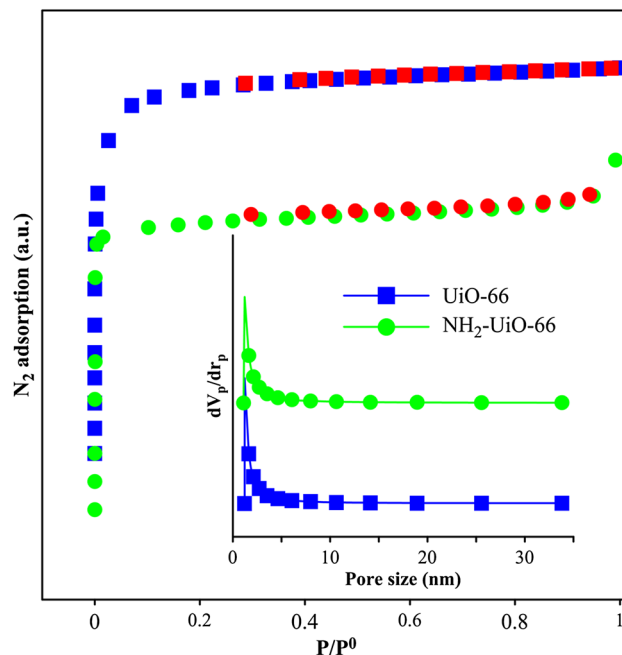


**Fig. 4** N<sub>2</sub> adsorption/desorption and pore size distribution of UiO-66 and NH<sub>2</sub>-UiO-66

### 3.1.3 TGA

The TGA was employed to check the thermal stability of UiO-66 and  $\text{NH}_2$ -UiO-66. The TGA and DTG curves in Fig. 3 show weight loss in three major steps. The first big weight loss (about 17% weight loss for UiO-66 and 22% for  $\text{NH}_2$ -UiO-66) occurs around 100 °C indicating the loss of surface water molecules. The second small weight loss (6–8% weight loss for UiO-66 and 3–5% for  $\text{NH}_2$ -UiO-66) around 200 °C corresponds to the loss of solvent (DMF) molecules from the pores, and also the loss of water molecules coordinated in the cage within MOFs. The third big weight loss observed around 540 and 350 °C for UiO-66 and  $\text{NH}_2$ -UiO-66, respectively, which are attributed to collapse the structure of MOFs and buried the organic linkers [37, 40].

### 3.1.4 BET

The specific surface area and pore volume of MOFs are the most important properties in adsorption application. The BET surface areas and pore size distribution of two samples were determined from the nitrogen adsorption/desorption isotherms at 77 K and the results presented in Fig. 4. It can be seen, that both samples have microporous structure. The BET surface areas and total pore volumes of two MOFs were calculated to be 1276  $\text{m}^2/\text{g}$  and 0.54  $\text{cm}^3/\text{g}$  for UiO-66, and 1258  $\text{m}^2/\text{g}$  and 0.51  $\text{cm}^3/\text{g}$  for  $\text{NH}_2$ -UiO-66. The specific surface areas and total pore volumes obtained in this study are higher than previously reported values [8], which can be due to smaller particle size and better activation. Probably the removal of unreacted reactants by

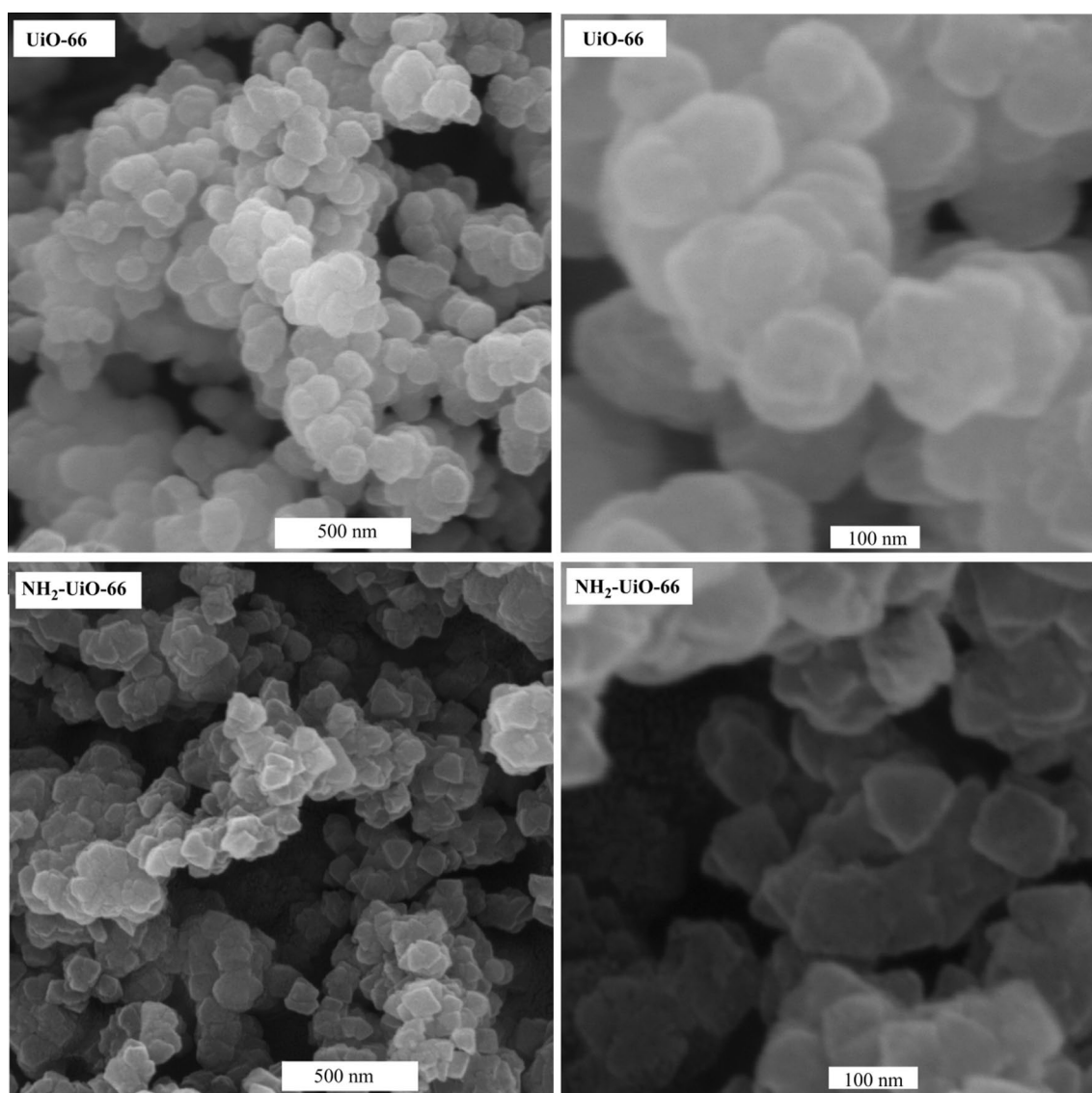


**Fig. 5** FESEM images of UiO-66 and  $\text{NH}_2$ -UiO-66

ultrasonic and used chloroform as exchanged solvent result high surface areas of MOFs.

### 3.1.5 SEM

The morphologies and particle sizes of MOFs were investigated by FESEM. FESEM images in Figure 5 showed regular shaped particles ranging from 100 to 1500 nm, much smaller than literature [38].  $\text{NH}_2\text{-UiO-66}$  displays symmetrical crystals with triangular base pyramid morphology, while UiO-66 displays round-shaped crystals; the crystal morphology of both MOFs synthesized in this study is similar with literature [38].

## 3.2 Comparison of the Antidotal Agents

### 3.2.1 Effect of the Different Drug to MOFs Ratio on Drug Adsorbance Efficiency of Antidotal Agents

Figure 6 shows adsorption isotherms of MTX adsorption over the two adsorbents. The MOFs adsorptions are evaluated after 2 h, and the results are compared in Table 1. The amount of adsorbed MTX with  $\text{NH}_2\text{-UiO-66}$  is slightly more than UiO-66 in the experimental conditions, which could be due to the formation of hydrogen bond between amine groups of  $\text{NH}_2\text{-UiO-66}$  and polar groups of MTX. When MTX concentration is about 0.48 mg/mL, adsorption capacity of UiO-66 and  $\text{NH}_2\text{-UiO-66}$  reaches to

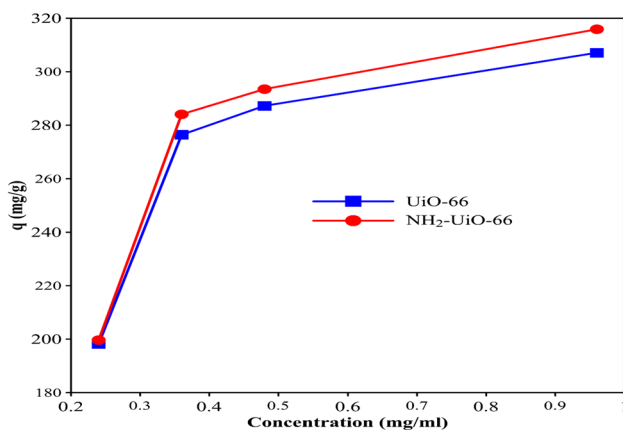


**Fig. 6** Drug adsorption curve

**Table 1** Adsorption table

Concentration (mg/mL)	0.24	0.36	0.48	0.96
q (mg/g)				
UiO-66	198.22	276.41	287.27	307.09
$\text{NH}_2\text{-UiO-66}$	199.66	284.09	293.51	315.87

maximum. The higher adsorption capacity of this MOFs for MTX, compared to other adsorbent agents, is probably because of the large porosity of MOFs because the adsorption capacity generally enhances with increasing the porosity of adsorbents [41, 42]. As Table 1 indicates, approximately both MOFs have same adsorption capacity. The maximum adsorption capacities for UiO-66 and  $\text{NH}_2\text{-UiO-66}$  are 307.09 and 315.87 mg/g, respectively. We supposed, the  $\pi\text{-}\pi$  stacking between amine group and MTX caused such a large adsorption capacity.

### 3.2.2 Adsorption Kinetics

Adsorption kinetics demonstrating the solute uptake rate is one of the most important characters which represents the adsorption efficiency of adsorbents and therefore determines their potential applications. The effect of contact time on the MTX adsorption on the both MOFs, at the initial concentrations of  $400\ \mu\text{g mL}^{-1}$  is shown in Fig. 7. The adsorption rate at the initial stage was very rapid for both MOFs. The time required to approach adsorption saturation is within 120 min, and further increase in the contact time did not lead to any noticeable adsorption. As we seen,  $q_e$  for  $\text{NH}_2\text{-UiO-66}$  is higher than UiO-66.

Some kinetic models such as the pseudo-first-order and pseudo-second-order were commonly used to simulate the adsorption kinetic data in liquid adsorption [43]. In this work, we tested both of these kinetic models, only the pseudo-second-order kinetic model can correlate the experimental dynamic data of MTX on both MOFs with

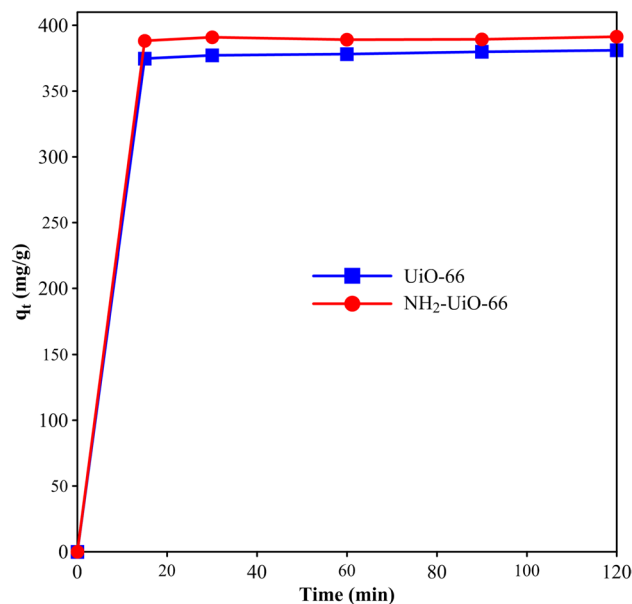


**Fig. 7** Effect of contact time on adsorption rate

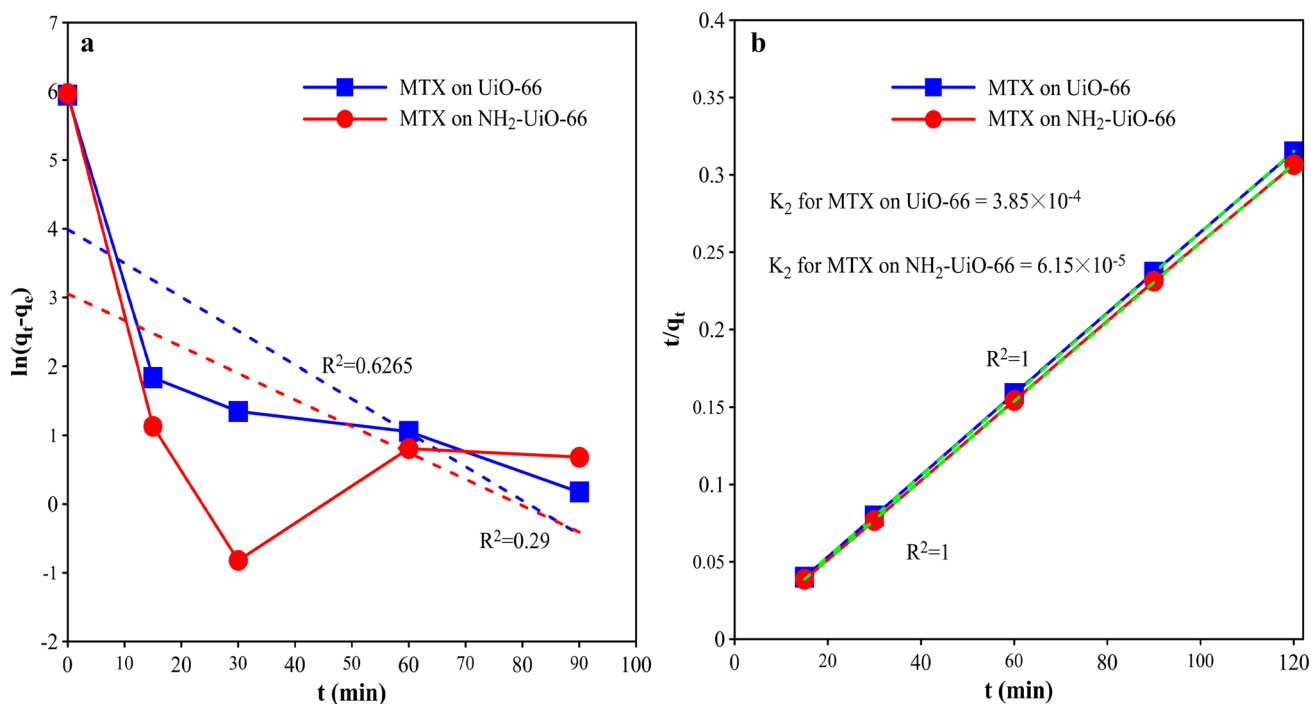


**Fig. 8** **a** Pseudo-first-order and **b** pseudo-second-order kinetic plots for MTX adsorption by MOFs

reasonable error. The pseudo-second-order kinetic model can be presented as [27]:

$$\frac{t}{q_t} = \frac{1}{K_2 q_e^2} + \frac{1}{q_e} t \quad (2)$$

where  $q_e$  and  $q_t$  are the amount of MTX (mg/g) adsorbed at equilibrium and at time  $t$ , respectively.  $k_2$  stands for the pseudo-second-order rate constant of adsorption (g/(mg min)) [44]. Linear plot feature of  $t/q_t$  versus  $t$  (Fig. 8) was achieved, and the  $k_2$  and  $R^2$  values calculated from the slopes are summarized in Table 2.

### 3.2.3 The Effect of Different Media on Interaction Between Mofs and Drug

In order to study the affinity between antidotal agents (MOFs) and drugs, the release study was evaluated on drug-adsorbed MOFs in neutral (pH 7.4) and acidified (pH 5.5) PBS solution (Fig. 9). Here, the two pH value were selected because pH 5.5 represents the endosomal pH of cells and pH 7.4 represents the physiological pH. The MTX release process from the MTX/MOFs was markedly prolonged compared with that of the MTX solution. Because of high solubility of MTX we guessed that drug release behavior of the MTX/MOFs to be sensitive to pH. But due to high affinity between MOFs and drugs pH sensitive behavior did not seen. The results exhibited, the rate of drug desorption/release were very slow at the both conditions. For example,

within 1 day, only about 11% and 9% MTX were desorbed from NH<sub>2</sub>-UiO-66 at pH 7.4 and 5.5, respectively. Also, after 96 h, cumulative release never exceeded over 12% at pH 7.4 and 5.5. These results proved that, both MOFs have approximately similar affinity to drug.

### 3.3 Cell Cytotoxicity of MOFs

Concerning the cytotoxicity of these porous compounds may be influenced by synthesis. The toxic properties of MOFs were investigated in HFF-2 cells because of their enriched neuritis which could reflect cells state and be observed easily [45]. MTT assay was conducted to measure the cell viability after introducing low- concentration of MOFs. As shown in Fig. 10, no significant growth inhibitions were observed with introducing of both of MOFs. With the increasing concentrations of MOFs (35, 70, 140, 280, 560 and 710 μg/mL), the cell viability remained around 80% at the maximum dosage after 48 h,

**Table 2** Kinetic Parameters for the Adsorption of MTX on MOFs at 310 K (37 °C) and initial concentration of 400 μg/mL

Adsorbent	$q_e$ (mg/g)	$k_2$ (g mg <sup>-1</sup> min <sup>-1</sup> )	$R^2$	
			First-order	Second-order
NH <sub>2</sub> -UiO-66	391.36	$6.15 \times 10^{-5}$	0.63	1.00
UiO-66	381.04	$3.85 \times 10^{-4}$	0.29	1.00

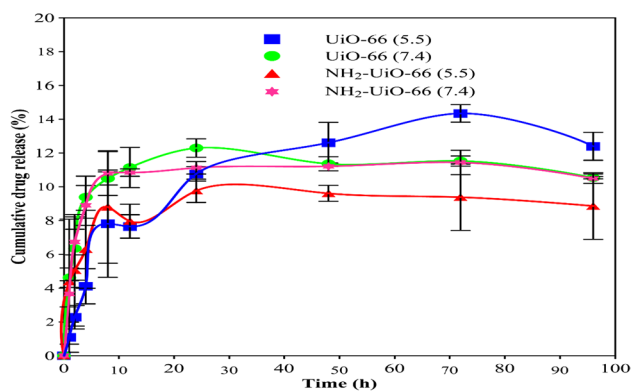


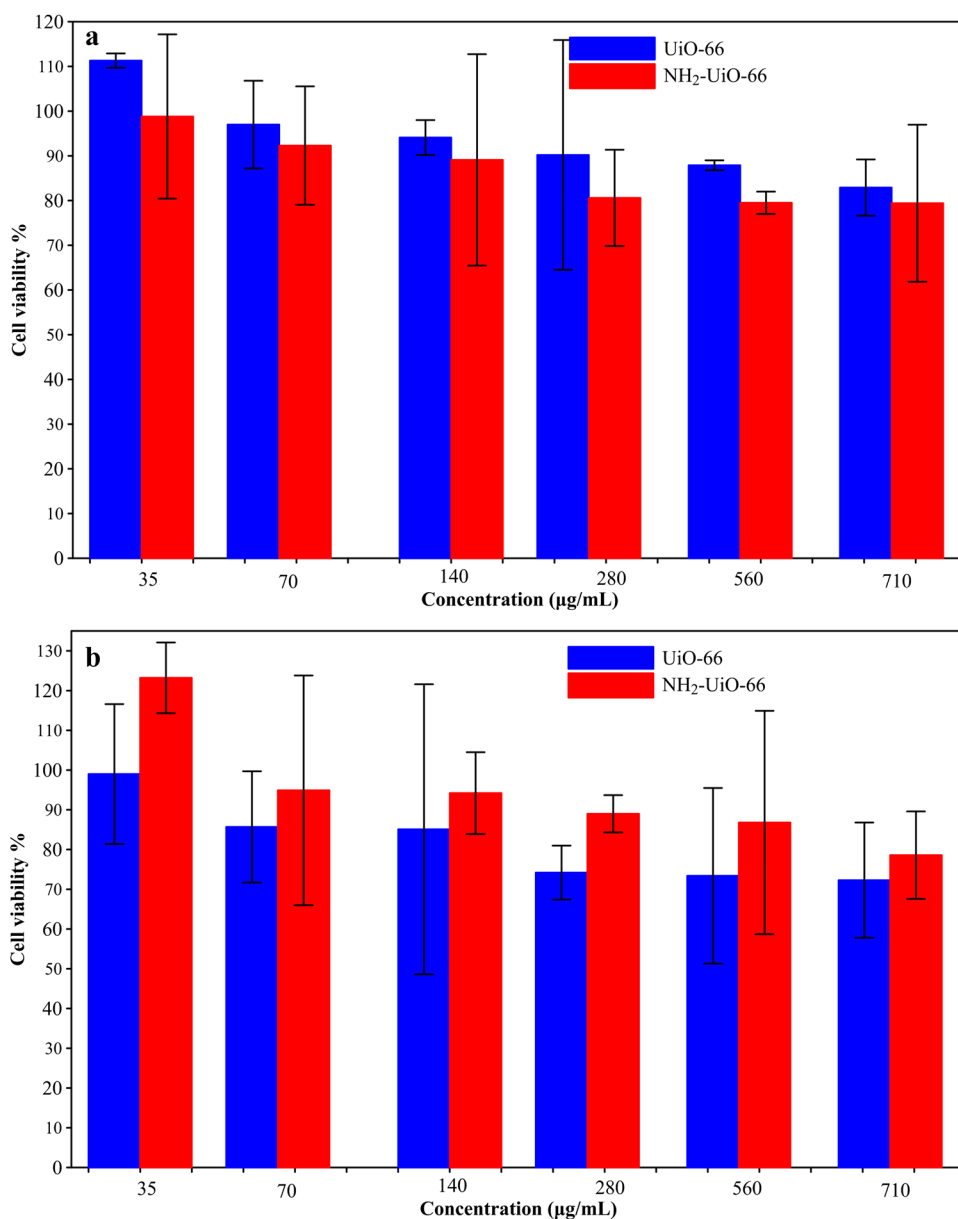
**Fig. 9** release curve of MOFs in various media

so, this observation indicating that UiO-based MOFs are a good antidote agent for adsorbing drug because of its low-toxicity.

#### 4 Conclusions

In summary, low cytotoxicity, MTX drug adsorbing capacity, high affinity and pH independent release of UiO-66 and NH<sub>2</sub>-UiO-66 were proved for ideal antidotal activity. The adsorption capacity for MTX with the UiO-66 and NH<sub>2</sub>-UiO-66 were approximately the same, and about 393.22 and 382.86 mg/g respectively. MTT assay results

**Fig. 10** Cell Cytotoxicity of MOFs after **a** 24 h and **b** 48 h





didn't showed significant decreased in the viability of cells even in the presence of 560 µg/mL MOFs. High affinity between MOFs and drug caused well efficacy of drugs adsorption such MTX.

**Acknowledgements** This study was supported financially by Zanjan University of medical science and Sharif University of Technology, Iran.

**Compliance with Ethical Standards**

**Conflict of interest** Authors declare no conflict of interest.

## References

- R.A. Rudd, Increases in drug and opioid-involved overdose deaths—United States, 2010–2015. *MMWR* **65**, 50–51 (2016)
- J. Mounteny et al., The drug situation in Europe: an overview of data available on illicit drugs and new psychoactive substances from European monitoring in 2015. *Addiction* **111**(1), 34–48 (2016)
- L.M. Meyer et al., Treatment of acute leukemia with amethopterin (4-amino, 10-methyl pteroyl glutamic acid). *Acta Haematol.* **4**(3), 157–167 (1950)
- B.F. Hoskins, R. Robson, Infinite polymeric frameworks consisting of three dimensionally linked rod-like segments. *J. Am. Chem. Soc.* **111**(15), 5962–5964 (1989)
- T. Yamada et al., Proton-conductive metal–organic frameworks. *Bull. Chem. Soc. Jpn.* **89**(1), 1–10 (2015)
- Y.-B. Huang et al., Multifunctional metal-organic framework catalysts: synergistic catalysis and tandem reactions. *Chem. Soc. Rev.* **46**, 126–157 (2017)
- B. Van de Voorde et al., Adsorptive separation on metal–organic frameworks in the liquid phase. *Chem. Soc. Rev.* **43**(16), 5766–5788 (2014)
- Q. Chen et al., Selective adsorption of cationic dyes by UiO-66-NH<sub>2</sub>. *Appl. Surf. Sci.* **327**, 77–85 (2015)
- C. Wang et al., Applications of water stable metal–organic frameworks. *Chem. Soc. Rev.* **45**(18), 5107–5134 (2016)
- N.S. Bobbitt et al., Metal–organic frameworks for the removal of toxic industrial chemicals and chemical warfare agents. *Chem. Soc. Rev.* (2017). doi:10.1039/c7cs00108h
- I. Erucar, S. Keskin, Computational investigation of metal organic frameworks for storage and delivery of anticancer drugs. *J. Mater. Chem. B* **5**(35), 7342–7351 (2017)
- J. Liu et al., Controllable porosity conversion of metal-organic frameworks composed of natural ingredients for drug delivery. *Chem. Commun.* **53**(55), 7804–7807 (2017)
- T. Sattar, M. Athar, Hydrothermal synthesis and characterization of copper glycinate (Bio-MOF-29) and its in vitro drugs adsorption studies. *Op. J. Inorg. Chem.* **7**(02), 17 (2017)
- S.E.H. Etaiw et al., Catalytic, Luminescence Activities and Structure of Metal-Organic Frameworks Containing CuCN Building Blocks and Bipodal Bridging Ligands. *J. Inorg. Organomet. Polym. Mater.* **21**(3), 465–475 (2011)
- S. Kitagawa, R. Kitaura, S.i. Noro, Functional porous coordination polymers. *Angew. Chem. Int. Ed.* **43**(18), 2334–2375 (2004)
- M. Eddaoudi et al., Systematic design of pore size and functionality in isoreticular MOFs and their application in methane storage. *Science* **295**(5554), 469–472 (2002)
- F. Li et al., Two Metal–organic frameworks with pharmaceutical ingredient linker: influence of pH and temperature. *J. Inorg. Organomet. Polym. Mater.* **27**(1), 334–341 (2017)
- A.R. Abbasi et al., Methyl orange removal from wastewater using [Zn<sub>2</sub>(oba)<sub>2</sub>(4-bpdh)] 3DMF metal–organic frameworks nanostructures. *J. Inorg. Organomet. Polym. Mater.* **25**(6), 1582–1589 (2015)
- N.A. Khan et al., Adsorption and removal of phthalic acid and diethyl phthalate from water with zeolitic imidazolate and metal–organic frameworks. *J. Hazard. Mater.* **282**, 194–200 (2015)
- M. Özacar, İ.A. Şengil, Adsorption of acid dyes from aqueous solutions by calcined alunite and granular activated carbon. *Adsorption* **8**(4), 301–308 (2002)
- B. Armağan, M. Turan, Equilibrium studies on the adsorption of reactive azo dyes into zeolite. *Desalination* **170**(1), 33–39 (2004)
- F. Rozada et al., Dye adsorption by sewage sludge-based activated carbons in batch and fixed-bed systems. *Bioresour. Technol.* **87**(3), 221–230 (2003)
- G. Annadurai, R.-S. Juang, D.-J. Lee, Use of cellulose-based wastes for adsorption of dyes from aqueous solutions. *J. Hazard. Mater.* **92**(3), 263–274 (2002)
- R. Mostafa Zamani, M. Rostami, M. Aghajanzadeh, H.K. Manjili, K. Rostamizadeh, H. Danafar, Mesoporous titanium dioxide@zinc oxide-graphene oxide nanocarriers for colon-specific drug delivery. *J. Mater. Sci.* (2017). doi:10.1007/s10853-017-1673-6
- H. Molavi et al., Enhancing CO<sub>2</sub>/N<sub>2</sub> adsorption selectivity via post-synthetic modification of NH<sub>2</sub>-UiO-66 (Zr). *Microporous Mesoporous Mater.* **257**, 193–201 (2018)
- A. Nematollahzadeh, A. Shojaei, M. Karimi, Chemically modified organic/inorganic nanoporous composite particles for the adsorption of reactive black 5 from aqueous solution. *React. Funct. Polym.* **86**, 7–15 (2015)
- M. Karimi, A. Nematollahzadeh, A. Shojaei, Amino functionalized hierarchically produced porous polyacrylamide microspheres for the removal of chromium (VI) from aqueous solution. *J. Porous. Mater.* (2017). doi:10.1007/s10934-017-0413-2
- H. Mahdavi, L. Ahmadian-Alam, H. Molavi, Grafting of sulfonated monomer onto an amino-silane functionalized 2-aminoterephthalate metal–organic framework via surface-initiated redox polymerization: proton-conducting solid electrolytes. *Polym. Int.* **64**(11), 1578–1584 (2015)
- H. Nosrati et al., Green and one-pot surface coating of iron oxide magnetic nanoparticles with natural amino acids and biocompatibility investigation. *Appl. Organomet. Chem.* (2017). doi:10.1002/aoc.4069
- H. Kheiri Manjili et al., Pharmacokinetics and in vitro and in vivo delivery of sulforaphane by PCL–PEG–PCL copolymeric-based micelles. *Artif. Cells Nanomed. Biotechnol.* **22**(8), 947–957 (2017)
- H. Danafar, Study of the composition of polycaprolactone/poly(ethylene glycol)/polycaprolactone copolymer and drug-to-polymer ratio on drug loading efficiency of curcumin to nanoparticles. *Jundishapur J. Nat. Pharm. Prod.* (2017). doi:10.5812/jjnpp.34179
- A. Nomani et al., Preparation and characterization of copolymeric polymersomes for protein delivery. *Drug Res.* **67**(08), 458–465 (2017)
- H. Danafar et al., Drug-conjugated PLA–PEG–PLA copolymers: a novel approach for controlled delivery of hydrophilic drugs by micelle formation. *Pharm. Dev. Technol.* **22**(8), 947–957 (2017). doi:10.3109/10837450.2015.1125920
- H. Danafar et al., Co-delivery of hydrophilic and hydrophobic drugs by micelles: a new approach using drug conjugated PEG–PCLNanoparticles. *Drug Dev. Ind. Pharm.* **43**(11), 1908–1918 (2017)

35. A. Sadeghi et al., Synthesis, characterization, and antibacterial effects of trimethylated and triethylated 6-NH<sub>2</sub>-6-deoxy chitosan. *J. Bioact. Compat. Polym.* **23**(3), 262–275 (2008)
36. H. Li et al., Design and synthesis of an exceptionally stable and highly porous metal-organic framework. *Nature* **402**(6759), 276 (1999)
37. J.H. Cavka et al., A new zirconium inorganic building brick forming metal organic frameworks with exceptional stability. *J. Am. Chem. Soc.* **130**(42), 13850–13851 (2008)
38. H.R. Abid et al., Adsorption of CH<sub>4</sub> and CO<sub>2</sub> on Zr-metal organic frameworks. *J. Colloid. Interface Sci.* **366**(1), 120–124 (2012)
39. H. Saleem, U. Rafique, R.P. Davies, Investigations on post-synthetically modified UiO-66-NH<sub>2</sub> for the adsorptive removal of heavy metal ions from aqueous solution. *Microporous Mesoporous Mater.* **221**, 238–244 (2016)
40. H.R. Abid et al., Amino-functionalized Zr-MOF nanoparticles for adsorption of CO<sub>2</sub> and CH<sub>4</sub>. *Int. J. Smart Nano Mater.* **4**(1), 72–82 (2013)
41. V. Fierro et al., Adsorption of phenol onto activated carbons having different textural and surface properties. *Microporous Mesoporous Mater.* **111**(1), 276–284 (2008)
42. E. Haque et al., Adsorption of phenol on mesoporous carbon CMK-3: effect of textural properties. *Bull. Korean Chem. Soc.* **31**(6), 1638–1642 (2010)
43. A. Gundogdu et al., Adsorption of phenol from aqueous solution on a low-cost activated carbon produced from tea industry waste: equilibrium, kinetic, and thermodynamic study. *J. Chem. Eng. Data* **57**(10), 2733–2743 (2012)
44. J. Hu et al., Removal of chromium from aqueous solution by using oxidized multiwalled carbon nanotubes. *J. Hazard. Mater.* **162**(2), 1542–1550 (2009)
45. M. Vicente et al., Synthesis, dark toxicity and induction of in vitro DNA photodamage by a tetra (4-nido-carboranylphenyl) porphyrin. *J. Photochem. Photobiol. B* **68**(2), 123–132 (2002)